Journal of Magnetic Resonance **149,** 74–84 (2001)
doi:10.1006/jmre.2000.2282, available online at http://www.idealibrary.com on IDEAL®

Electron Spin Relaxation Time Measurements Using Radiofrequency Longitudinally Detected ESR and Application in Oximetry

Ioannis Panagiotelis, Ian Nicholson, and James M. S. Hutchison

Department of Biomedical Physics and Bio-Engineering, University of Aberdeen, Foresterhill, Aberdeen AB25 2ZD, United Kingdom

Received September 11, 2000; revised December 18, 2000

Longitudinally detected ESR (LODESR) involves transverse ESR irradiation with a modulated source and observing oscillations in the spin magnetization parallel to the main magnetic field. In this study, radiofrequency-LODESR was used for oximetry by measuring the relaxation times of the electron. T_{1e} and T_{2e} were measured by investigating LODESR signal magnitude as a function of detection frequency. We have also predicted theoretically and verified experimentally the LODESR signal phase dependence on detection frequency and relaxation times. These methods are valid even for inhomogeneous lines provided that $T_{1e} \gg T_{2e}$. We have also developed a new method for measuring T_{1e}, valid for inhomogeneous spectra, for all values of T_{1e} and T_{2e}, based on measuring the spectral area as a function of detection frequency. We have measured T_{1e} and T_{2e} for lithium phthalocyanine crystals, for the nitroxide TEMPOL, and for the single line agent Triarylmethyl (TAM). Furthermore, we have collected spectra from aqueous solutions of TEMPOL and TAM at different oxygen concentrations and confirmed that T_{1e} values are reduced with increased oxygen concentration. We have also measured the spin–lattice electronic relaxation time for degassed aqueous solutions of the same agents at different agent concentrations. T_{1e} decreases as a function of concentration for TAM while it remains independent of free radical concentration for TEMPOL, a major advantage for oxygen mapping. This method, combined with the ability of LODESR to provide images of exogenous free radicals *in vivo*, presents an attractive alternative to the conventional transverse ESR linewidth based oximetry methods.

Key Words: **LODESR; oximetry; electron relaxation times**; ***in vivo*** **EPR; inhomogeneous broadening.**

INTRODUCTION

Free radicals play an important role in the progression of many diseases and physiological processes. ESR techniques can detect unpaired electrons of free radicals directly (*1, 2*) and perform an indirect assessment of pO_2, microviscosity, and pH *in vivo* by means of measurements of certain spectral parameters such as electron relaxation times and hyperfine constants (*3, 4*). These applications are of particular clinical interest in providing noninvasive, repetitive, rapid, sensitive, and quantitative measurements (*5*). Oxygen partial pressure is a very important parameter in most metabolic processes. Furthermore, certain drugs have different pharmacological effects depending on the local pO_2 and pH (*6*). Recent advances in ESR combined with new insights and information from cell and molecular biology mean that critical determinants for diagnosis and therapy can now be probed. Physiological and metabolic measurements can provide a means for optimization of therapy for individual patients.

A paramagnetic sample behaves nonlinearly when irradiated by electromagnetic radiation with two frequencies in the neighborhood of the resonance frequency (ω_0) (*7*). Irradiation of the spin system by two different but close frequencies, ω_1 and ω_2, is equivalent to irradiation with a single frequency at $(\omega_1 + \omega_2)/2\,(=\omega_0)$ that is sinusoidally modulated at a much lower frequency, $(\omega_1 - \omega_2)/2$ [1], (*8*):

$$\cos\omega_1 t + \cos\omega_2 t = 2 \cdot \cos\left[\frac{\omega_1 - \omega_2}{2}\right]t \cdot \cos\left[\frac{\omega_1 + \omega_2}{2}\right]t. \quad [1]$$

Longitudinally detected ESR (LODESR) involves continuous, transverse ESR irradiation with a modulated source. The signal is detected from oscillations in the spin magnetization parallel to the main magnetic field. The M_z oscillations are detected with a coil tuned to $\Omega = (\omega_1 - \omega_2)$, placed parallel to the main field. Spectra are collected by sweeping the main field to cover the resonance. It has been demonstrated that RF-LODESR (300 MHz) is capable of detecting free radicals with concentrations on the order of micromolar from aqueous samples (*9*). Furthermore, RF-LODESR spectra and images have been obtained *in vivo* in the rat following administration of nitroxide free radicals such as PCA (2,2,5,5-tetramethyl pyrrolidine-1-oxyl-3-carboxylic acid) (*10*). The theoretical sensitivity limit of RF-LODESR is lower than for standard RF-ESR with transverse detection for the same excitation frequency (*11*). RF-LODESR, however, has many advantages for biological samples. The dominant noise source in RF-LODESR is the thermal noise of the detection coil with a very small contribution from the first amplification stage (*9*). Additionally in LODESR, due to the low detection frequency, the resonant properties of the detection coil are not significantly affected by animal cardiac and respiratory motion (*9, 10, 12–14*). LODESR does not suffer from power limitations due to frequency modulation noise (*7*). The applied power is determined by the saturation properties of the sample (*9*). Finally, LODESR has increased spectral resolution for samples containing more

1090-7807/01 $35.00

than one species of spin system (*15*). This is of particular importance *in vivo*, where the superimposition of broad and narrow lines is common.

For solutions of free radicals, measurements of ESR spectral linewidth contain information on the electron spin–spin relaxation time, T_{2e}. Extraction of this information, however, is complicated because the lineshape depends on many parameters including concentration changes, hyperfine coupling of the electron with surrounding nuclei, and instrumental sources of line broadening (*16*). The distribution of a free radical agent *in vivo* leads to differential bioreduction of the agent (*17, 18*). The extraction of information from T_{2e} can therefore only be qualitative since the linewidth is influenced by local spin probe concentration. Additionally, the correction for inhomogeneous broadening effects requires excellent signal-to-noise-ratio (SNR) and sophisticated spectral analysis techniques (*16, 19, 20*). The spin–lattice relaxation time of the electron, T_{1e}, is less dependent on concentration changes (*21, 22*) and can be obtained independently from inhomogeneous broadening effects using LODESR (*23, 24*). T_{1e} based techniques have another inherent advantage; generally T_{1e} is greater than T_{2e}, particularly for slow motion molecular dynamics, as observed in many biological applications (*25*). The main interaction between the oxygen molecules and the paramagnetic agent in solution is Heisenberg spin exchange, which broadens the ESR linewidth and consequently reduces T_{2e} (*5*). Oxygen increases the coupling of free radical energy states to the lattice, leading to increased probability of electron relaxation and shortening of the relaxation times (*25*). The percentage of change in T_{1e} is much greater as a function of oxygen than that of T_{2e} in biological samples, where the rotational correlation time increases (*25*).

The current methods for electron spin–lattice relaxation time measurement present certain difficulties that hinder their application. Progressive power saturation involves measuring the EPR signal height as a function of incident microwave power (*26*). It measures an effective T_{1e} that corresponds to the sum of all relaxation pathways, therefore influenced by hidden processes (*27, 28*). Furthermore, the most significant error is introduced by inaccurate conversion of the power incident on the resonator into excitation field strength values, B_1. It is also limited to T_{1e} values longer than 10^{-7} s (*29*). Excessive RF-power dissipation heats the sample, affecting T_{1e} with increasing temperature. Similar problems are involved in an analogue to the progressive saturation technique, where T_{1e} is obtained by analyzing the dynamic nuclear polarization enhancement curve as a function of the saturating magnetic field (*30*).

Time domain techniques such as saturation recovery and electron spin echo at radiofrequencies (*22, 31*) are restricted to measuring relaxation times longer than 10^{-6} s. Most investigations are limited to very low temperatures where the relaxation times are usually longer. Additionally, low quality factors are required for the resonators (reducing sensitivity) in order to reduce ringdown overloading (*23*). At RF frequencies, e.g., 300 MHz, the receiver dead time is around 425 ns (*32*). Relaxation time measurements from spins with T_{2e} less than 1 μs (nitroxides) are therefore not yet feasible. X-band LODESR has been used to measure T_{1e}, overcoming the above problems (*23, 24, 33–35*). T_{1e} was determined from measuring LODESR signal as a function of modulation frequency. T_{1e} values ranging from 10^{-5} to 10^{-10} s can be determined (*29*).

In this study, RF-longitudinally detected ESR was used for oximetry by measuring the electronic spin–lattice relaxation time T_{1e}. T_{1e} was measured by investigating LODESR signal magnitude, phase, and spectral area as a function of the detection frequency. Phase is defined as the angle between the applied modulated excitation and the oscillation of the longitudinal magnetization (M_z) (*7*). We measured T_{1e} initially for lithium phthalocyanine (LiPc) crystals (gifted by Prof. Walzack, Dartmouth College, NH). We have also measured T_{1e} as a function of agent concentration for the nitroxide TEMPOL (4-hydroxy-2,2,6,6-tetra-methyl-piperidine-1-oxy, Sigma-Aldrich Co. Ltd.) and the single line agent triarylmethyl (TAM OX063, Nycomed Innovations, Malmö, Sweden). We have collected spectra from aqueous solutions of TEMPOL and TAM at different oxygen concentrations and measured spin–lattice electronic relaxation times, confirming that T_{1e} as well as T_{2e} values are reduced with increased oxygen concentration.

THEORY

Several investigators have studied the dependence of the amplitude of the longitudinal magnetization on detection frequency. Colligiani *et al.* (*23*), using a quantum mechanical approach, obtained the following expression for the component of the magnetization oscillating at $\Omega = |(\omega_i - \omega_j)|$ (not the actual signal induced in the detection coil) in the case of spin $1/2$:

$$\overline{S_{\mathrm{LOD}}(\Omega)} \propto \frac{1}{\frac{i}{T_{1e}} + \Omega}\left[\frac{\omega_i}{\frac{i}{T_{2e}} + (\omega_0 - \omega_i)} + \frac{\omega_j}{\frac{i}{T_{2e}} + (\omega_0 - \omega_j)}\right], \quad [2]$$

where ω_i and ω_j are the angular frequencies of the two irradiating waves. The main assumption for the validity of the above expression was that $\alpha \ll 1$, where α is the saturation factor (given by $\alpha = \gamma_e B_1^2 T_{1e} T_{2e}$, where γ_e is the gyromagnetic ratio for the electron and B_1 is the RF excitation field). The M_z oscillation amplitude corresponding to expression [2] is shown in Fig. 1. The amplitude of the fundamental oscillation is plotted as a function of the magnetic field and the detection frequency Ω. When Ω is increased, spins fail to follow the rapid modulation, leading to a decrease of the amplitude of the oscillations of the longitudinal magnetization and subsequent reduction of the LODESR signal (*29*). For the spins to follow the oscillation of the RF-excitation field, T_{1e} must be significantly shorter than one period of oscillation (*8*). Another significant observation is that the width of the LODESR spectrum increases as a function of detection

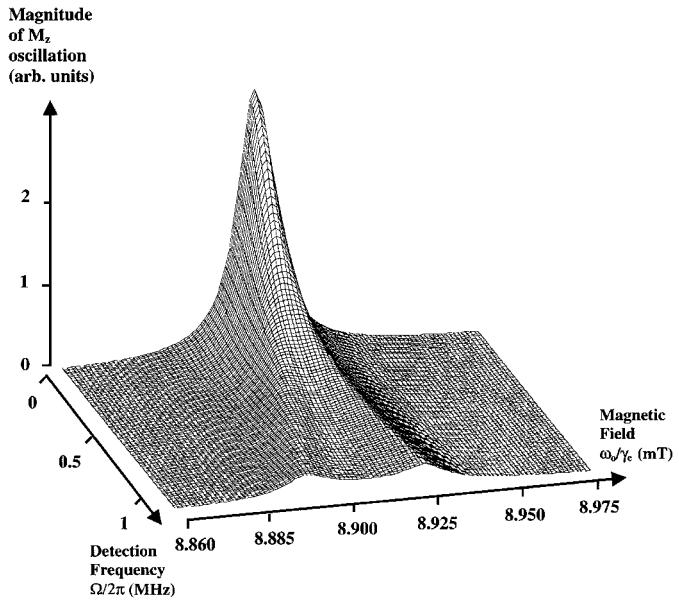

FIG. 1. The longitudinal magnetization (M_z) oscillation magnitude, corresponding to expression [2], as a function of the magnetic field and the detection frequency Ω, for $T_{1e} = T_{2e} = 1\ \mu$s.

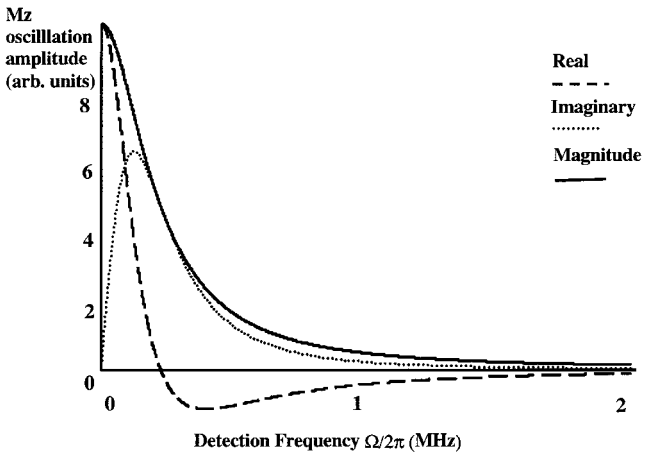

FIG. 2. The longitudinal magnetization (M_z) oscillation magnitude, corresponding to expression [4], as a function of detection frequency, Ω, together with the real and imaginary components, derived from expression [2], for $T_{1e} = T_{2e} = 1\ \mu$s.

frequency and eventually it becomes double peaked. LODESR is a multiphoton phenomenon (*23*). As the detection frequency increases, the two Lorentzians (represented by the terms in square brackets in [2]) become clearer and can eventually be resolved. In the case where $T_{1e} \gg T_{2e}$, as observed in solids or for liquids with very slow molecular dynamics, the part of [2] containing the T_{2e} terms remains almost constant as a function of Ω with respect to the T_{1e} term and [2] can be approximated by [3] (*23, 36*).

$$\overline{S_{\mathrm{LOD}}(\Omega)} \propto \frac{1}{\frac{i}{T_{1e}} + \Omega} \qquad [3]$$

Substituting in [2], $\omega_i = \omega_0 - \Omega/2$ and $\omega_j = \omega_0 + \Omega/2$ (*37*), the magnitude of [2] is given by

$$|S_{\mathrm{LOD}}(\Omega)| = K \cdot \frac{T_{1e} \cdot T_{2e}}{\sqrt{\left(1 + \Omega^2 \cdot T_{1e}^2\right) \cdot \left(1 + \Omega^2 \cdot T_{2e}^2/4\right)}}, \qquad [4]$$

where K is a proportionality factor. Figure 2 shows a graph of $|S_{\mathrm{LOD}}(\Omega)|$, together with the real and imaginary components as a function of detection frequency, derived from expression [2]. The LODESR signal has also been calculated by Bassompierre and Pescia (*38*) using the density matrix evolution equation and by Herve (*33*) using the Bloch equations reaching a similar formula. Leporini (*36*) proposed a theory that extends the result of the linear response theory (which relates the susceptibility to the Laplace transforms of proper relaxation functions), also including nonlinear susceptibilities. The theory takes into full account the quantum-mechanical character of the spin-radiation interaction and the formulae are identical with those mentioned above.

The phase of the oscillating component of M_z depends on static magnetic field, relaxation times, modulation frequency, and power of irradiation (*7*). For the same power level and field value, the phase response to modulation frequency depends only on relaxation times. Again, by substituting in [2], $\omega_i = \omega_0 - \Omega/2$ and $\omega_j = \omega_o + \Omega/2$, the expression for the LODESR phase as a function of detection frequency can be calculated as

$$\theta(\Omega) = \tan^{-1}\left(\Omega \cdot \frac{2 \cdot T_{1e} + T_{2e}}{2 - \Omega^2 \cdot T_{1e} \cdot T_{2e}}\right). \qquad [5]$$

There is an apparent phase transition where the real part of the signal changes sign (Fig. 3). This corresponds to $\theta = \pm\pi/2$,

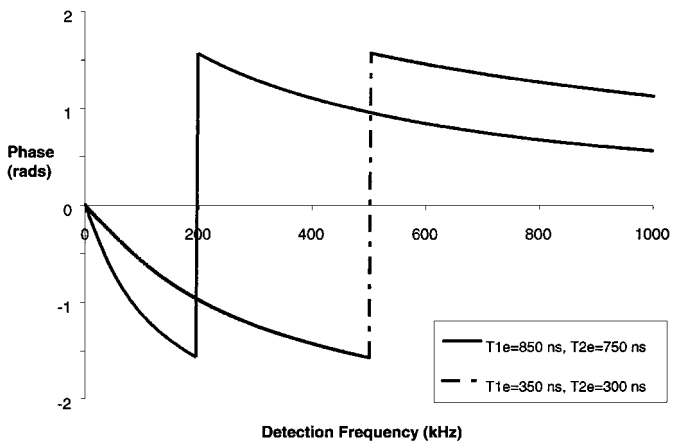

FIG. 3. The M_z oscillation phase, corresponding to expression [5], as a function of detection frequency Ω. For the solid line $T_{1e} = 850$ ns and $T_{2e} = 750$ ns, while for the dotted line $T_{1e} = 350$ ns and $T_{2e} = 300$ ns.

at which point the denominator of the argument of [5] is zero, hence

$$\Omega_C = \sqrt{\frac{2}{T_{1e} \cdot T_{2e}}}. \quad [6]$$

Equation [5] provides another useful method for measuring relaxation times. LODESR phase has also been used by Atsarkin *et al.* (*39, 40*), but only to measure spin–lattice relaxation in the case $T_{1e} \gg T_{2e}$. Both expressions [4] and [5] are valid for both homogeneous and inhomogeneous lines in the case $T_{1e} \gg T_{2e}$. The inhomogeneous broadening can be attributed to many spin ensembles in the same spin system that have Larmor frequencies ω_0^*, slightly different from each other, according to a specific distribution (usually Gaussian) which depends on the environment (*19*). The modulus of the M_z oscillation amplitude is given by the convolution of the LODESR function [2] for a homogeneous line with the distribution function (*23, 24*)

$$\overline{S_{LOD}(\Omega)} \propto \int d\omega_0^* F(\omega_0^*) \frac{1}{\frac{i}{T_{1e}} + \Omega} \times \left[\frac{\omega_i}{\frac{i}{T_{2e}} + (\omega_0^* - \omega_i)} + \frac{\omega_j}{\frac{i}{T_{2e}} + (\omega_0^* - \omega_j)} \right], \quad [7]$$

where $F(\omega_0^*)$ is the Larmor frequency distribution function of the spin ensembles. We have assumed this function to be a Gaussian (*19*):

$$g(\omega_0^*) = \exp\left[-\frac{1}{2} \left(\frac{\omega_0^* - \omega_0}{w_g} \right)^2 \right], \quad [8]$$

where w_g is the FWHM of the Gaussian curve.

The different spin ensembles contribute to the amplitude of the LODESR signal and not to the width of the resonance, provided that $T_{1e} \gg T_{2e}$ over the range of detection frequencies of about $\pm 3/T_{1e}$ (*23, 24*). Under these conditions the integral of the part of expression [7] in square brackets, involving the T_{2e} and the ω_0^* terms, remains constant as a function of detection frequency.

LODESR therefore directly gives T_{1e} even in the case of inhomogeneous broadened lines and accounts for the relaxation times of the single spin packet when all spectral components have the same T_{1e} value (*24*). LODESR, in the case of many spin species in the sample, accounts for the mean T_{1e} value. In particular, when two different T_{1e} values are present, the curve corresponding to the LODESR signal as a function of detection frequency is the superimposition of two curves, each one corresponding to a different T_{1e} (*29*).

The convolution of functions [2] and [8] is equivalent, in the frequency domain, to the product of the Fourier transforms of these two functions (*41*). Applying the Fourier transform on the real part of expression [2] gives

$$F_{REAL}(k) = C_R \cdot \left[\frac{(\omega_i - \omega_j)}{\frac{1}{T_{1e}^2} + (\omega_i - \omega_j)^2} \left[-i \cdot \omega_i \cdot \pi \cdot e^{-i \cdot k \cdot \omega_i} \cdot e^{\frac{k}{T_{2e}}} + i \cdot \omega_j \cdot \pi \cdot e^{-i \cdot k \cdot \omega_j} \cdot e^{\frac{k}{T_{2e}}} \right] + \frac{1}{T_{1e} \cdot \left[\frac{1}{T_{1e}^2} + (\omega_i - \omega_j)^2 \right]} \cdot \left[-\omega_i \cdot \pi \cdot e^{-i \cdot k \cdot \omega_i} \cdot e^{\frac{k}{T_{2e}}} - \omega_j \cdot \pi \cdot e^{-i \cdot k \cdot \omega_j} \cdot e^{\frac{k}{T_{2e}}} \right] \right], \quad [9]$$

where k is the angular wavenumber (units of time) and C_R is a proportionality constant. The above calculation was performed with Mathcad (Mathsoft, Inc., Cambridge, MA) symbolic processor. Only negative k-values were used because of symmetry. Applying the Fourier transform on the imaginary part of expression [2] gives

$$F_{IMAG}(k) = C_I \cdot \left[\frac{(\omega_i - \omega_j)}{\frac{1}{T_{1e}^2} + (\omega_i - \omega_j)^2} \left[-\omega_i \cdot \pi \cdot e^{-i \cdot k \cdot \omega_i} \cdot e^{\frac{k}{T_{2e}}} - \omega_j \cdot \pi \cdot e^{-i \cdot k \cdot \omega_j} \cdot e^{\frac{k}{T_{2e}}} \right] - \frac{1}{T_{1e} \cdot \left[\frac{1}{T_{1e}^2} + (\omega_i - \omega_j)^2 \right]} \cdot \left[-i \cdot \omega_i \cdot \pi \cdot e^{-i \cdot k \cdot \omega_i} \cdot e^{\frac{k}{T_{2e}}} + i \cdot \omega_j \cdot \pi \cdot e^{-i \cdot k \cdot \omega_j} \cdot e^{\frac{k}{T_{2e}}} \right] \right] \quad [10]$$

Again, C_I is a proportionality constant. The Fourier transform of expression [8] is

$$F_{Gaussian} = \sqrt{2 \cdot \pi} \cdot w_g \cdot e^{-\left(\frac{1}{2} k^2 \cdot w_g^2 + i \cdot k \cdot \omega_0 \right)}. \quad [11]$$

The product of [9] and [11] is equivalent to the Fourier transform of the convolution of the Gaussian function with the real part of [2].

$$F_{Gaussreal} = F_{Gaussian} \times F_{REAL}. \quad [12]$$

Accordingly, the product of [10] and [11] is equivalent to the Fourier transform of the convolution of the Gaussian function with the imaginary part of [2].

$$F_{Gaussimag} = F_{Gaussian} \times F_{IMAG}. \quad [13]$$

Expressions [12] and [13] are complex functions. By separating real and imaginary parts and then substituting $k = 0$ (in order to get the DC level of the Fourier transforms), the imaginary

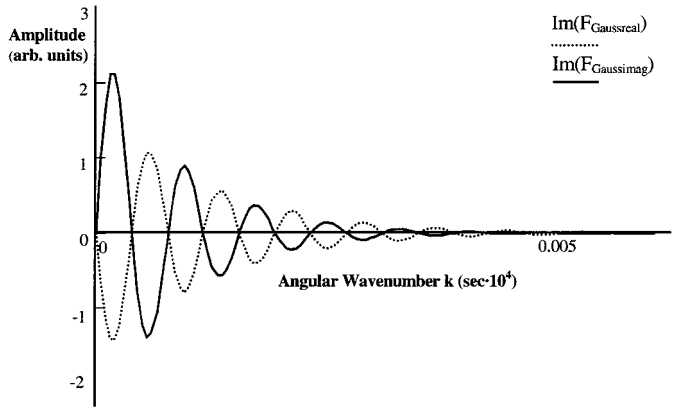

FIG. 4. Imaginary parts of expressions [13] and [14] for $T_{1e} = 500$ ns and $T_{2e} = 100$ ns. The imaginary parts are zero for $k = 0$ (DC level).

parts of [12] and [13] become zero (Fig. 4). By substituting $\omega_i = \omega_0 - \Omega/2$ and $\omega_j = \omega_0 + \Omega/2$ on the real part of [12], we have

$$F^{k=0}_{\text{Gaussreal}} = 2 \cdot \sqrt{2} \cdot \pi^{\frac{3}{2}} \cdot \omega_0 \cdot w_g \cdot \frac{T_{1e}}{\left(\Omega^2 \cdot T_{1e}^2 + 1\right)}. \quad [14]$$

Accordingly, [14] gives

$$F^{k=0}_{\text{Gaussimag}} = 2 \cdot \sqrt{2} \cdot \pi^{\frac{3}{2}} \cdot \omega_0 \cdot w_g \cdot \frac{T_{1e}^2}{\left(\Omega^2 \cdot T_{1e}^2 + 1\right)}. \quad [15]$$

The function that gives the total DC level of the LODESR convolved function [7] is given by the vectorial sum of expressions [14] and [15]:

$$F^{k=0}_{\text{total}} = 2 \cdot \sqrt{2} \cdot \pi^{\frac{3}{2}} \cdot \omega_0 \cdot w_g \cdot \frac{T_{1e}}{\sqrt{\Omega^2 \cdot T_{1e}^2 + 1}}. \quad [16]$$

Equation [16] can be rewritten as

$$F^{k=0}_{\text{total}} = C \cdot \frac{T_{1e}}{\sqrt{\Omega^2 \cdot T_{1e}^2 + 1}}. \quad [17]$$

Equation [17] gives the DC level of the Fourier transform of the total convoluted LODESR function (which is the area under the LODESR spectrum) as a function of detection frequency (Ω) and T_{1e}. The Gaussian width parameter w_g and the central Larmor frequency (ω_0) are incorporated in the constant of proportionality C. Equation [17] is the same relationship to Ω, as given by Eq. [4] for homogeneous lines or inhomogeneous lines when $T_{1e} \gg T_{2e}$. The importance of Eq. [17] stems from the fact that by measuring the LODESR spectral area as a function of detection frequency we can derive the electron spin–lattice relaxation time (T_{1e}) independently from inhomogeneous broadening, without any restriction for the relationship between T_{1e} and T_{2e}.

The LODESR spectral area corresponds to the total number of spins that participate in the LODESR phenomenon. In an attempt to interpret expression [17], as Ω increases, the probability that the spins will be excited decreases and the population difference in the spin system decreases. T_{1e} determines the time, Δt, a given spin spends in a state (spin lifetime-T_{2e} independent). The probability that a spin will participate in the resonance decreases as the period of the oscillating exciting field τ ($\tau = 1/\Omega$) is getting significantly shorter than Δt, $\tau \ll \Delta t$.

EXPERIMENTAL

LODESR spectra were collected using a coil assembly consisting of a birdcage excitation coil and a solenoidal receiver coil, shown in Fig. 5. ESR excitation was applied via a Six-leg, high-pass birdcage coil of 7.5-cm length and 3.8-cm diameter. The coil was tuned to 250 MHz, with a Q of 145 (matched to 50 Ω), which was reduced to 57 when loaded with saline of physiological concentration. The solenoidal signal detection coil consisted of 116 turns of 0.44-mm-thick, enamel-coated copper wire, wound onto a 2.6-cm-diameter plastic tube, to a length of 2.2 cm. The solenoid was tuned to cover a range of detection frequencies from 70 kHz to 1 MHz, in 12 steps, in order to cover a range of detection frequencies. The detection frequency had to change in a discrete manner so that we always measured the LODESR signal at resonance of the detection circuitry. This was achieved by selecting the appropriate tuning capacitors in the detection circuit by a rotary switch. The LODESR excitation frequency was 250 MHz, mixed with a frequency ranging from 35 to 500 kHz. The Q values of the solenoidal coil (not matched at 50 Ω) at each detection frequency are shown in Table 1. All spectra were collected at power levels well below saturation and did not exceed 0.5 W.

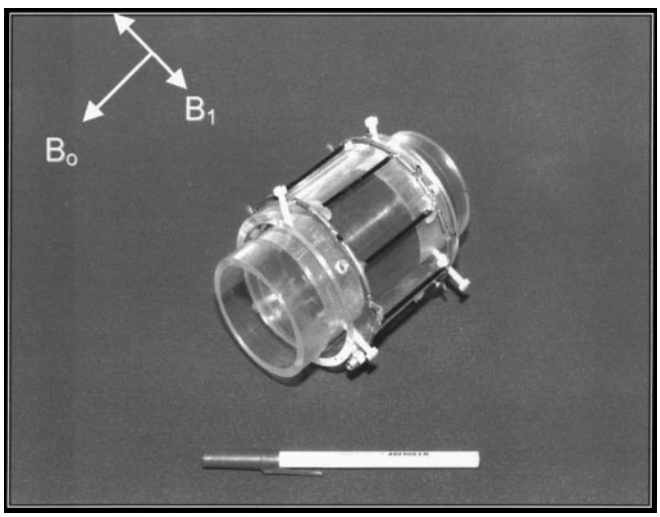

FIG. 5. Photograph of the LODESR RF-coil assembly. B_0 is the direction of the swept field and B_1 is the direction of the field produced by the birdcage resonator.

TABLE 1
Q-Values for the Solenoidal Coil as a Function of Detection Frequency

Detection frequency (kHz)	Q
70	26
100	40
160	58
270	66
350	74
410	84
490	94
570	98
640	104
740	108
810	120
970	150

Note. Q-values of the solenoidal detection coil (not matched to 50 Ω), as measured at each of the 12 detection frequencies. At these low frequencies Q-values are not significantly affected when the coil is loaded with a physiological saline sample.

The RF-coil assembly was placed inside the main (in-house) magnet, formed from an air-cored Helmholtz pair of coils of 20-cm internal diameter, with a 5.4-cm axial gap. The (in-house) magnet power supply was computer controlled and swept over a range from 6 to 12 mT in several seconds to collect the LODESR spectra. Figure 6 shows a block diagram of the system. The outputs of two signal generators (FLUKE 6060B and Stanford Research Systems DS345) were intermodulated by a double balanced modulator (minicircuits ZAD-1) to produce the modulated signal which was then amplified by a wide-band RF amplifier (KALMUS 118C) before coupling to the birdcage coil. The irradiation power was measured using a 20-dB directional coupler (minicircuits ZFDC-20-1H) and an inline power meter (Bird Electronic Corp., Thruline 4391 A). The signal induced in the detection coil was measured using a pair of homebuilt preamplifiers. The first stage incorporated a J-FET feedback preamplifier that employs negative feedback, giving effective detection coil Q-values around 7, while maintaining the signal-to-noise ratio of the undamped coil (*42*). This approach was mainly adapted in order to avoid using another set of capacitors in order to match the solenoidal coil at each detection frequency. The amplified signal was then applied to a pair of demodulators which are operated in quadrature (90° phase difference), forming the x and y channels of detection. It was then digitized and stored in a computer (Acorn A5000). Colligiani *et al.* suggested the use of analogic multiplexers in order to insert the appropriate capacitor in the resonant circuit (*23*), but this idea was abandoned since the resistance introduced (∼40 ohm) was unacceptable and would substantially reduce the Q factor of the resonator.

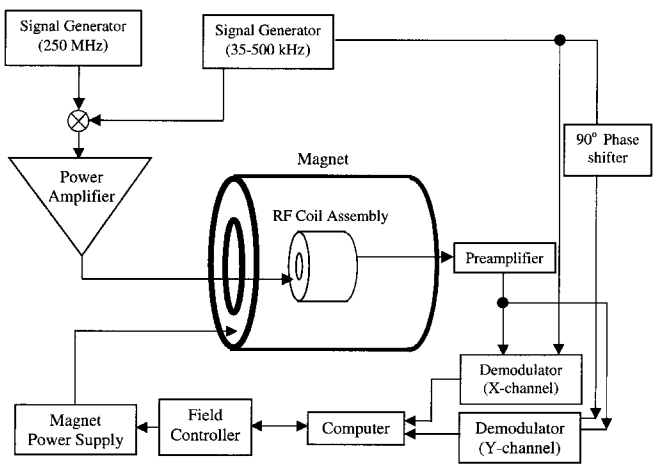

FIG. 6. Block diagram of the LODESR system.

Calibration of the frequency response of the detection apparatus was performed using a solid DPPH (1-1-diphenyl-2-picrylhydrazyl, Sigma-Aldrich Co. Ltd.) sample, whose ESR relaxation times are known to be $T_{1e} = T_{2e} = 67$ ns (*43*). T_{1e} and T_{2e} were then calculated by fitting the experimental data to the theoretical lines with Mathcad, by means of the iterative Levenberg–Marquardt algorithm (*44*). All spectra were collected at controlled temperature by means of a temperature controller (RS CAL-9000). In-phase and quadrature spectra were recorded against detection frequency. M_z oscillation magnitude, phase, and spectral areas were derived using macros built in Excel (Microsoft Corp.).

In practice, the spectral area is not immediately derived from Eq. [17], due to the fact that the two channels of detection do not necessarily coincide with the real or imaginary data. In particular the area represented by expression [17] is given by

$$A = \sqrt{A_R^2 + A_I^2}, \qquad [18]$$

where

$$A_R = \int S_R \cdot d\Omega \qquad [19]$$

and

$$A_I = \int S_I \cdot d\Omega, \qquad [20]$$

where S_R and S_I are the real and imaginary components of the M_z oscillation. Considering the phase difference between the x channel of the detection circuitry and the real axes to be equal to ϕ, we have

$$S_R = S_X \cdot \cos\phi - S_Y \cdot \sin\phi \qquad [21]$$

and

$$S_I = S_X \cdot \sin\phi + S_Y \cdot \cos\phi, \qquad [22]$$

where S_X and S_Y are the components of the M_z oscillation in

the x and y channels of the detection circuitry. Substituting [21] and [22] in [19] and [20], respectively, we find

$$A = \sqrt{A_R^2 + A_I^2} = \sqrt{A_X^2 + A_Y^2}. \quad [23]$$

So A can be measured by taking the vectorial sum of the spectral areas from each channel of the detection circuitry.

The samples for oximetry were prepared by bubbling different O_2/N_2 gas mixtures through the sample for 45 min (*45*). The oxygen concentration of the samples after gas bubbling was measured using a Clark-type polarographic electrode (Lazar Research Labs, Inc., DO-166-NP Micro pO_2 Needle Probe).

RESULTS AND DISCUSSION

Relaxation times were measured initially on a sample of lithium phthalocyanine, using LODESR oscillation magnitude as a function of detection frequency. LiPc crystals are water insoluble and not easily biodegraded. The linewidth is very dependent on oxygen tension and has a pure Lorentzian lineshape. These properties are very useful for quantitative oxygen measurements (*46, 47*). The sample was deoxygenated, sealed in a glass tube, and kept at room temperature (24°C). The spectra were collected using 14 mW of irradiation power. A typical spectrum collected is shown in Fig. 7. The theoretical line corresponding to expression [4] was fitted optimally to the experimental data, as shown in Fig. 8. The fitting parameters were $T_{1e} = 934 \pm 66$ ns and $T_{2e} = 653 \pm 46$ ns. LiPc expresses a pure homogeneous line and the FWHM of the LODESR absorption spectrum is 18 ± 1 μT, which corresponds to a T_{2e} of 631 ± 35 ns. A similar value was also obtained by Alecci (*48*) for a similar sample, measured with RF-EPR.

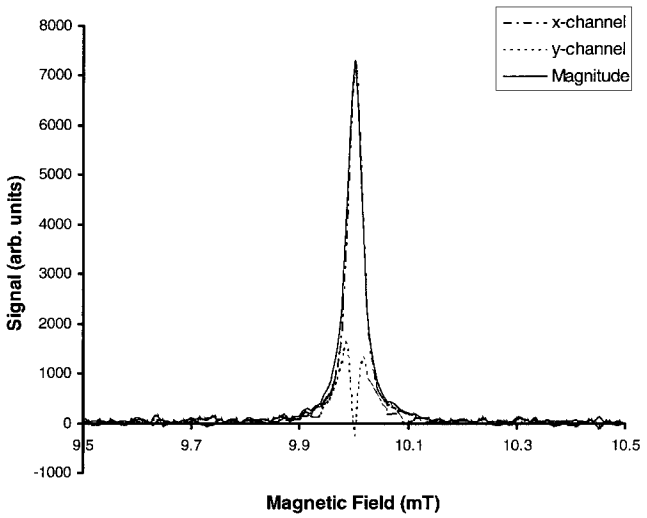

FIG. 7. LODESR spectrum collected from a degassed LiPc sample at 160 kHz, at room temperature (24°C), with a 1-mT field sweep, 12-s sweep time, 50-ms time constant, 1 average, and 20-mW input power.

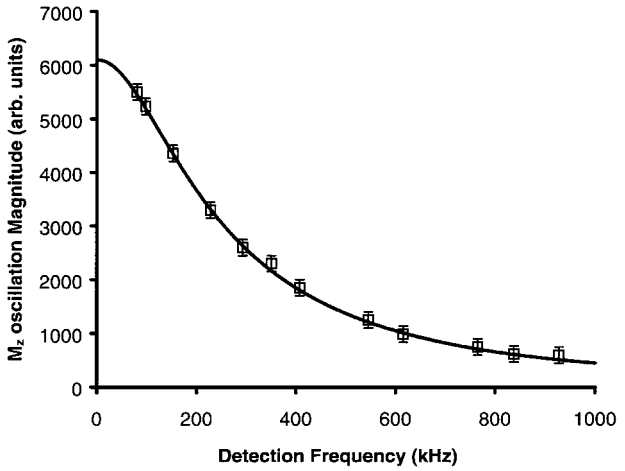

FIG. 8. LODESR signal magnitude as a function of detection frequency (Ω) from LiPc in N_2 atmosphere. The theoretical line (solid line) corresponding to expression [4] was fitted optimally with the experimental data when $T_{1e} = 934 \pm 66$ ns and $T_{2e} = 653 \pm 46$ ns.

We also measured relaxation times for a 1 mM aqueous solution of triarylmethyl, measuring the LODESR signal phase and spectral area as a function of detection frequency. TAM is a stable, water soluble, paramagnetic agent exhibiting a single, narrow ESR line and has particularly good properties for oximetry (*30*). The ratio of the Gaussian to Lorentzian linewidths for the degassed solution at infinite dilution is 3.3 (*30*). The sample was equilibrated with 100% oxygen gas (37 ± 2 mg/l dissolved $[O_2]$) and it was kept at 37°C (for future comparisons *in vivo*). The spectra were collected at 150 mW irradiation power. A typical spectrum collected is shown in Fig. 9. The theoretical line

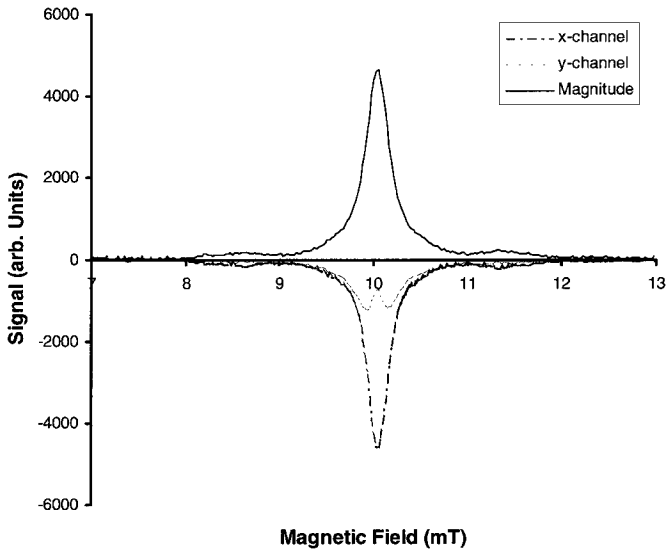

FIG. 9. LODESR spectrum collected from a 1 mM aqueous solution of TAM equilibrated with pure oxygen at 740 kHz, at 37°C, with a 2-mT field sweep, 14-s sweep time, 50-ms time constant, 1 average, and 150-mW input power.

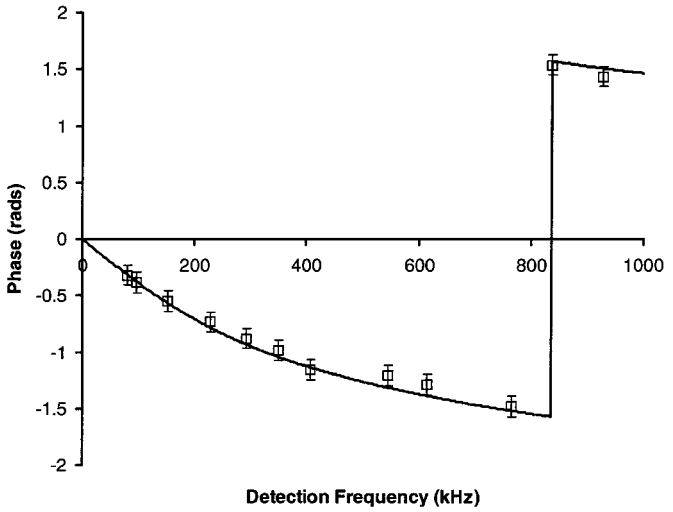

FIG. 10. LODESR signal phase as a function of detection frequency, Ω, from a 1 mM aqueous solution of TAM equilibrated with pure oxygen. The theoretical line (solid) corresponding to expression [5] was fitted optimally with the experimental data when $T_{1e} = 580 \pm 32$ ns and $T_{2e} = 125 \pm 21$ ns.

corresponding to LODESR phase as a function of Ω (expression [5]) was fitted optimally to the experimental data, as shown in Fig. 10, resulting in the parameter values $T_{1e} = 580 \pm 32$ ns and $T_{2e} = 125 \pm 21$ ns. TAM expresses a predominantly homogeneous line at this oxygen concentration and FWHM of the LODESR absorption spectrum is 102 ± 1 μT, which corresponds to a T_{2e} of 111 ± 23 ns. The theoretical line corresponding to LODESR spectral area as a function of Ω (expression [17]) was fitted optimally to the experimental data (Fig. 11), giving $T_{1e} = 573 \pm 35$ ns. This value is the same within experimental uncertainties with that measured using the LODESR phase approach.

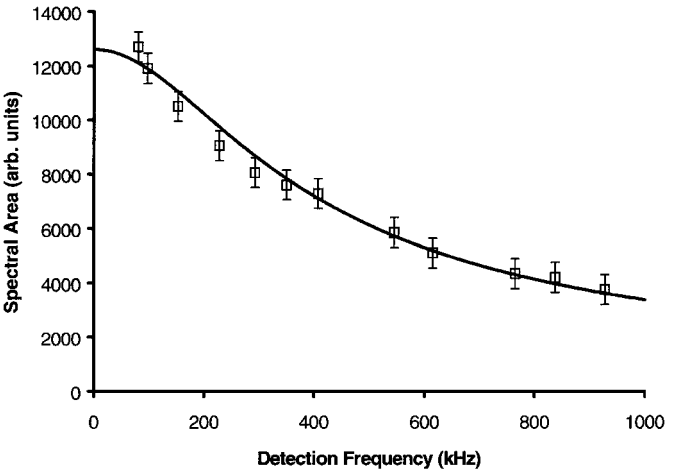

FIG. 11. LODESR spectral area as a function of detection frequency, Ω, from a 1 mM aqueous solution of TAM equilibrated with pure oxygen. The theoretical line (solid line) corresponding to expression [18] was fitted optimally with the experimental data when $T_{1e} = 573 \pm 35$ ns.

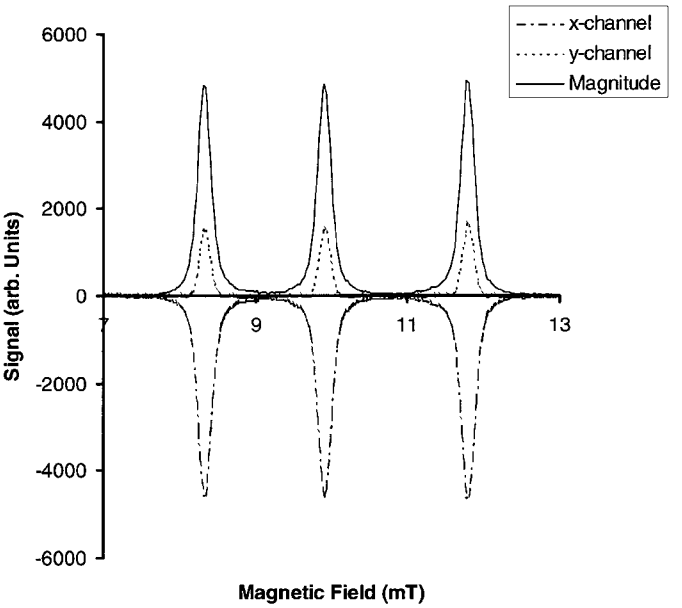

FIG. 12. LODESR spectra collected from 1 mM degassed TEMPOL in deionized water at 740 kHz, at 37°C, with a 6-mT field sweep, 12-s sweep time, 50-ms time constant, 1 average, and 350-mW input power.

We have also measured T_{1e} as a function of agent concentration for aqueous solutions of TEMPOL and triarylmethyl (TAM OX063). The samples were kept at 37°C throughout the experiments and oxygen concentration for the degassed solutions was measured with the Clark electrode as 0.3 mg/L dissolved oxygen (5 mm Hg pO_2). Typical spectra collected are shown in Figs. 12 and 13. T_{1e} was measured using the spectral area as a function

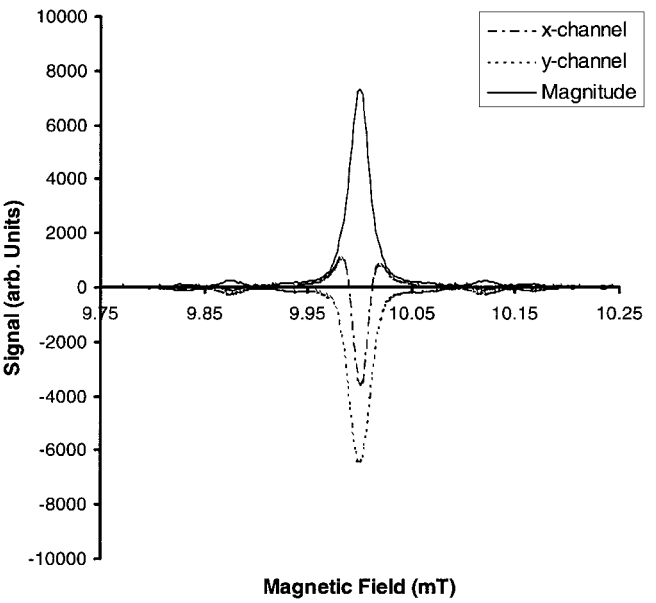

FIG. 13. LODESR spectra collected from 1 mM degassed TAM in deionized water at 160 kHz, at 37°C, with a 0.5-mT field sweep, 28-s sweep time, 50-ms time constant, 1 average, and 50-mW input power.

of detection frequency approach, which is valid even in the case of inhomogeneously broadened lines such as those from TEMPOL and TAM. The results are shown in Fig. 14. For TAM the longitudinal relaxation rate (T_{1e}^{-1}) changes linearly as a function of concentration at a rate of $0.031 \pm 0.004\ \mu s^{-1}\ mM^{-1}$. TAM is a large ionic molecule and the dominant relaxation mechanism between like spins of TAM in aqueous solutions is from dipole–dipole interactions (*30, 49*). Dipolar interactions are effective spin–lattice relaxation mechanisms and their effectiveness increases as a function of agent concentration (*50*).

On the other hand, T_{1e} for TEMPOL solutions is constant as a function of concentration, within experimental errors. TEMPOL is a small neutral molecule and the dominant relaxation mechanism between like spins in aqueous solutions of TEMPOL is Heisenberg spin exchange (*49*). In this case, T_{1e} is independent of free radical concentration changes because spin exchange interactions, which occur between free radical molecules, only result in transfer of magnetization between the hyperfine lines (loss of phase coherence) and not in transfer of energy to the lattice (*21, 22, 25*).

This result favors the use of TEMPOL in comparison with TAM for *in vivo* applications since, generally, free radical agents have differential distribution in various tissues as a result of metabolism to nonparamagnetic derivatives, excretion, distribution to different temperature, and microviscosity areas, or attachment to macromolecules within the course of the experiment (*18*).

We have also measured spin–lattice electronic relaxation times for 1 mM aqueous solutions of TAM and TEMPOL at different oxygen concentrations. T_{1e} values were obtained again by measuring the LODESR spectral area as a function of detection frequency. The spectra were collected at 37°C and the power input was well below saturation levels (saturation factor, $\alpha \sim 0.08$). The results are shown in Fig. 15. The oxygen longitudinal relaxivity for TEMPOL was measured as $6.726 \pm 0.590\ \mu s^{-1}\ mM^{-1}$ while for TAM it was measured as $2.256 \pm 0.718\ \mu s^{-1}\ mM^{-1}$. The percentage of change, however, between the values of longitudinal relaxation rate obtained under anoxic and aerated conditions, is 290 and 679% for TEMPOL and TAM, respectively.

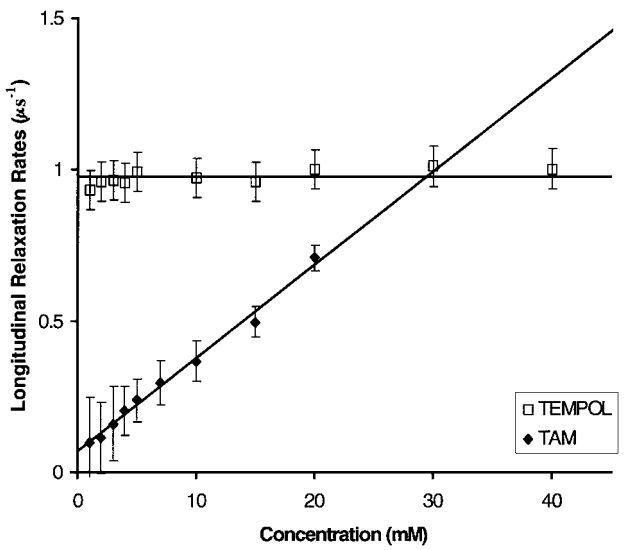

FIG. 14. Longitudinal relaxation rates as a function of agent concentration, from degassed aqueous solutions of TEMPOL and TAM. The solid lines represent linear regression fits.

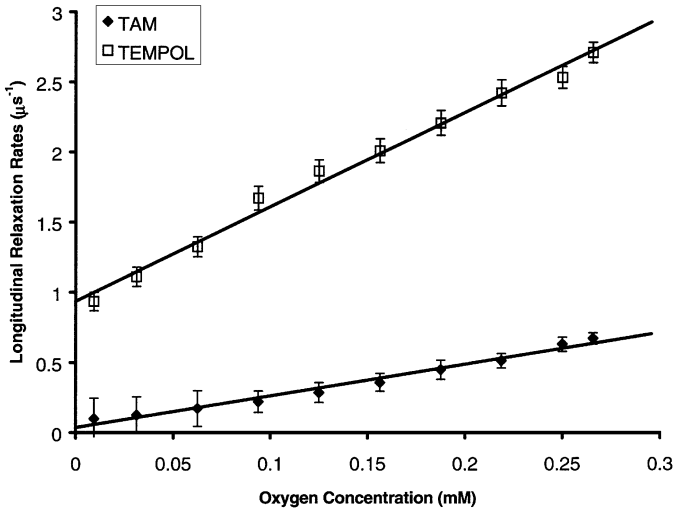

FIG. 15. Longitudinal relaxation rates as a function of dissolved oxygen concentration from 1 mM aqueous solutions of TEMPOL and TAM. The solid lines represent linear regression fits.

CONCLUSIONS

We have performed relaxation time measurements using continuous wave RF-LODESR. T_{1e} and T_{2e} values were obtained by measuring the magnitude, phase, and area of the LODESR spectrum as a function of detection frequency. The results are valid in the case of inhomogeneously broadened lines for all approaches when $T_{1e} \gg T_{2e}$. For the approach involving the measurement of spectral areas, T_{1e} values are valid in the case of inhomogeneously broadened lines without any restriction on the relationship between T_{1e} and T_{2e}. The main advantages of T_{1e} relaxometry were described and *in vitro* oximetry was performed. Measuring oxygen *in vivo*, independent from free radical concentration changes and inhomogeneously broadened lines, is an attractive perspective. There is no need to use spectral analysis to disentangle these effects, decreasing the overall processing time and the *in vivo* related artifacts. The above, combined with the ability of RF-LODESR to provide images of exogenous free radicals *in vivo* (*10*), results in a powerful technique that can perform accurate, localized, noninvasive measurements of T_{1e} and T_{2e}.

Relaxation time measurements could be performed by selecting a region of interest on a series of LODESR images collected

at different detection frequencies. T_{1e} and T_{2e} could then be measured using the signal magnitude and phase approaches. Calibration for the decrease of signal intensity due to biological clearance would not be required when using the signal phase approach. The spectral areas approach would require spectral–spatial imaging. The oxygen relaxivity of the agents is expected to change *in vivo* due to the higher viscosity and due to binding with macromolecules. T_{1e} as a function of pO_2 calibration tables must be developed to correspond to *in vivo* situations.

In the future we intend to investigate the feasibility of *in vivo* T_{1e}-weighted LODESR imaging or T_{1e}-mapping in order to achieve oxygen mapping. This would require the development of software that will allocate relaxation time values for each particular pixel. Combined applications with NMR (*51*) increase the potential of the technique, allowing simultaneous collection of functional and anatomical information.

ACKNOWLEDGMENTS

The authors acknowledge Prof. T. Walczack, Dartmouth College, New Hampshire, for supplying the lithium phthalocyanine sample. We are also grateful to Dr J. H. Ardenkjær-Larsen and Nycomed Innovations, Malmö, Sweden, for supplying the triarylmethyl (TAM OX 063) agent.

REFERENCES

1. H. Yokoyama, Y. Lin, O. Itoh, Y. Ueda, A. Nakajima, T. Ogata, T. Sato, H. Ohya-Nishiguchi, and H. Kamada, EPR imaging for *in-vivo* analysis of the half-life of a nitroxide radical in the hippocampus and cerebral cortex of rats after epileptic seizures, *Free Rad. Biol. Med.* **27** (3/4), 442–448 (1999).
2. K. L. Chan, X. H. Zhang, P. C. W. Fung, W. H. Guo, and P. K. H.Tam, Role of nitric oxide in intestinal ischaemia–reperfusion injury studied using electron paramagnetic resonance, *B. J. Surg.* **86,** 1427–1432 (1999).
3. H. M. Swartz, S. Boyer, P. Gast, J. F. Glockner, H. Hu, K. J. Liu, M. Moussavi, S. W. Norby, N. Vahidi, T. Walczack, M. Wu, and R. B. Clarkson, Measurements of pertinent concentrations of oxygen *in-vivo*, *Magn. Reson. Med.* **20,** 333–339 (1991).
4. A. Sotgiu, K. Mäder, G. Placidi, S. Colacicchi, C. L. Ursini, and M. Alecci, pH-sensitive imaging by low-frequency EPR: A model study for biological applications, *Phys. Med. Biol.* **43,** 1921–1930 (1998).
5. H. M. Swartz and R. B. Clarkson, The measurement of oxygen *in-vivo* using EPR techniques, *Phys. Med. Biol.* **43,** 1957–1975 (1998).
6. K. Mäder, Pharmaceutical applications of *in vivo* EPR, *Phys. Med. Biol.* **43,** 1931–1935 (1998).
7. M. Giordano, G Ranieri and L. Pardi, Nuclear double resonance by longitudinal detection, *J. Magn. Reson.* **30,** 27–32 (1978).
8. H. Mchaurab and J. Hyde, Dependence of the multiple-quantum EPR signal on the spin–lattice relaxation time. Effect of oxygen in spin-labeled membranes, *J. Magn. Reson. B* **101,** 178–184 (1993).
9. I. Nicholson, F. J. L. Robb, and D. J. Lurie, Imaging paramagnetic species using radiofrequency longitudinally detected ESR (LODESR Imaging), *J. Magn. Reson. B* **104,** 284–288 (1994).
10. I. Nicholson, M. A. Foster, F. J. L. Robb, J. M. S. Hutchison, and D. J. Lurie, *In vivo* imaging of nitroxide-free-radical clearance in the rat, using radiofrequency longitudinally detected ESR imaging, *J. Magn. Reson. B* **113,** 256–261 (1996).
11. A. Schweiger and R. R. Ernst, Pulsed ESR with longitudinal detection. A novel recording technique, *J. Magn. Reson.* **77,** 512–523 (1988).
12. H. Yokoyama, T. Sato, N. Tsuchihashi, T. Ogata, H. Ohya-Nishiguchi, and H. Kamada, A CT using longitudinally detected ESR (LOESR-CT) of intraperitoneally injected nitroxide radical in a rat's head, *Magn. Reson. Imag.* **15,** 6, 701–708 (1997).
13. H. Yokoyama, T. Sato, T. Ogata, H. Ohya-Nishiguchi, and H. Kamada, *In-vivo* longitudinally detected ESR measurements at microwave regions of 300, 700, and 900 MHz in rats treated with a nitroxide radical, *J. Magn. Reson.* **129,** 201–206 (1997).
14. T. Sato, H. Yokoyama, H. Ohya-Nishiguchi, and H. Kamada, Measuring method of longitudinally detected ESR signal intensities against resonant frequencies at 250 to 950 MHz in a constant microwave field, *Appl. Magn. Reson.* **16,** 33–43 (1999).
15. M. Martinelli, L. Pardi, C. Pinzino, and S. Santucci, Dependence on relaxation times of longitunally detected paramagnetic resonance, *Solid State Commun.* **17,** 211–212 (1975).
16. B. Robinson, C. Mailer, and A. W. Reese, Linewidth analysis of spin labels in liquids. I. Theory and data analysis, *J. Magn. Reson.* **138,** 199–209 (1999), doi: jmre.1999.1737.
17. H. Halpern, M. Peric, T. Nguyen, D. P. Spencer, B. Teicher, Y. Lin, and M. Bowman, Selective isotopic labelling of a nitroxide spin label to enhance sensitivity for T_2 oxymetry, *J. Magn. Reson.* **90,** 40–51 (1990).
18. H. Halpern, C. Yu, M. Peric, E. Barth, D. J. Grdina and B. Teicher, Oxymetry deep in tissues with low-frequency electron paramagnetic resonance, *Proc. Natl. Acad. Sci. USA* **91,** 13047–13051 (1994).
19. B. Bales, Correction for inhomogeneous line broadening in spin labels, II, *J. Magn. Reson.* **48,** 418–430 (1982).
20. T. I. Smirnova, A. I. Smirnov, R. B. Clarkson, and R. L. Belford, Accuracy of oxygen measurements in T_2 (line width) EPR oximetry, *Magn. Reson. Med.* **33,** 801–810 (1995).
21. J. Yin, M. Paseikiewicz-Gierula, and J. S. Hyde, Lateral diffusion of lipids in membranes by pulse saturation recovery electron spin resonance, *Proc. Natl. Acad. Sci. USA* **84,** 964–968 (1987).
22. P. W. Percival and J. S. Hyde, Saturation-recovery measurements of the spin–lattice relaxation times of some nitroxides in solution, *J. Magn. Reson.* **23,** 249–257 (1976).
23. A. Colligiani, M. Giordano, D. Leporini, M. Lucchesi, M. Martinelli, L. Pardi, and S. Santucci, Longitudinally detected electron spin resonance: Recent developments, *Appl. Magn. Reson.* **3,** 107–129 (1992).
24. D. Leporini, "Non Linear Electron Spin Resonance in Liquid and Amorphous Systems," Ph.D. thesis, Dipartmento di Fisica, Pisa, Italy (1987).
25. J. S. Hyde and W. K. Subczynski, Spin-label oximetry, in "Biological Magnetic Resonance, Vol. 8, Spin Labelling, Theory and Applications", (L. J. Berliner and J. Reuben, Eds.), pp. 399–425, Plenum, New York (1989).
26. D. A. Haas, C. Mailer, and B. H. Robinson, Using nitroxide spin labels. How to obtain T_{1e} from continuous wave electron paramagnetic resonance spectra at all rotational rates, *Biophys. J.* **64,** 594–604 (1993).
27. F. Cianflone, F. Francia, and D. Leporini, Measurement of the longitudinal relaxation time by continuous-wave, nonlinear electron spin resonance spectroscopies, *J. Magn. Reson.* **131,** 86–91 (1998).
28. B. H. Robinson, D. A. Haas, and C. Mailer, Molecular dynamics in liquids: Spin–lattice relaxation of nitroxide spin labels, *Science* **263,** 490–493 (1994).
29. J. Pescia, MW AM in EPR, and short T_1 measurement, in "Foundations of Modern EPR" (G. R. Eaton, S. S. Eaton, and K. M. Salikhov, Eds.), pp. 768–780, World Scientific, Singapore (1998).
30. J. H. Ardenkjær-Larsen, I. Laursen, I. Leunbach, G. Ehnholm, L.-G. Wistrand, J. S. Petersson, and K. Golman, EPR and DNP properties of certain novel single electron contrast agents intended for oximetric imaging, *J. Magn. Reson.* **133,** 1–12 (1998).
31. L. Banci, I. Bertini, and C. Luchinat, "Nuclear and Electron Relaxation," VCH, Weinheim, Germany (1991).

32. N. Devasahayam, S. Subramanian, R. Murugesan, J. A. Cook, M. Afeworki, R. G. Tschudin, J. B. Mitchell, and M. C. Krishna, Parallel coil resonators for time-domain radiofrequency electron paramagnetic resonance imaging of biological objects, *J. Magn. Reson.* **142,** 168–176 (2000), doi:jmre.1999.1926.

33. J. Herve, Measurement of electronic spin–lattice relaxation times by rapid modulation of the saturation factor, in "Paramagnetic Resonance," (W. Low, Ed.), pp. 689–697, Academic Press, San Diego (1963).

34. J. Pescia, La mesure des temps de relaxation spin-réseau trés courts, *Ann. Phys.* **10,** 389–406 (1965).

35. J. Herve and J. Pescia, Resonance paramagnetique—Mesure du temps de relaxation T_1 par modulation du champ radiofrequence H_1 et détection de la variation d' aimantation selon le champ directeur, *C. R. Ac. Sci.* **251,** 665–667 (1960).

36. D. Leporini, Relationship between a nonlinear response and relaxation induced by a colored noise, *Phys. Rev. A* **49**(2), 992–1014 (1994).

37. M. Giordano, M. Martinelli, L. Pardi, S. Santucci, and C. Umeton, Variable frequency experiments in electron spin double resonance by a longitudinal detection, *J. Magn. Reson.* **64,** 47–60 (1985).

38. A. Bassompierre and J. Pescia, Magnétisme.–Théorie de la résonance paramagnétique en présence d'un champ radiofréquence modulé en amplitude, *C. R. Ac. Sci.* **254,** 4439–4441 (1962).

39. V. A. Atsarkin, V. V. Demidov, and G. A. Vasneva. Electron-spin–lattice relaxation in $GdBa_2Cu_3O_{6+x}$, *Phys. Rev. B* **52**(2), 1290–1296 (1995).

40. V. A. Atsarkin, V. V. Demidov, and G. A. Vasneva. Electron spin–lattice relaxation in noncommon metals $Yba_2Cu_3O_x$ and Rb_1C_{60}, *Appl. Magn. Reson.* **15,** 323–331 (1998).

41. G. Folland, "Fourier Analysis and Its Applications," Mathematics Series Wadsworth & Brooks/Cole, Belmont, CA (1992).

42. D. I. Hoult, Fast recovery, high sensitivity NMR probe and preamplifier for low frequencies, *Rev. Scient. Instrum.* **50**(2), 193–200 (1979).

43. N. Bloembergen and S. Wang, Relaxation effects in para- and ferromagnetic resonance, *Phy. Rev.* **93**(1), 72–83 (1954).

44. W. T. Vetterling, W. H. Press, S. A. Teukolsky, and B. P. Flannery, "Numerical Recipes in C," Cambridge Univ. Press, Cambridge, UK (1988).

45. I. B. Butler, M. A. A. Schoonen, and D. T. Rickard, Removal of oxygen from water: A comparison of four common techniques, *Talanta* **41**(2), 211–215 (1994).

46. M. Afeworki, N. R. Miller, N. Devasahayam, J. Cook, J. B. Mitchell, S. Subramanian, and M. C. Krishna, Preparation and EPR studies of lithium phthalocyanine radical as an oxymetric probe, *Free Rad. Med. Biol.* **25**(1), 72–78 (1998).

47. K. J. Liu, P. Gast, M. Moussavi, S. W. Norby, N. Vahidi, T. Walczak, M. Wu, and H. M. Swartz, Lithium phthalocyanine: A probe for electron paramagnetic resonance oximetry in viable biological systems, *Procl. Natl. Acad. Sci. USA Biophysics.* **90,** 5438–5442 (1993).

48. M. Alecci, "New Magnetic Resonance Techniques for *in Vivo* Free Radical Detection," Ph.D. thesis, University of Aberdeen, Aberdeen, UK (1998).

49. D. Marsh, Experimental methods in spin–label spectral analysis, in "Biological Magnetic Resonance, Vol. 8, Spin Labelling, Theory and Applications" (L. J. Berliner and J. Reuben, Eds.), pp. 255–304, Plenum, New York (1989).

50. J. S. Hyde, H. M. Swartz, and W. E. Antholine, The spin-probe-spin-label method, in "Spin Labelling II, Theory and Applications" (L. Berliner, Ed.), pp. 71–113 (1979).

51. I. Nicholson, F. J. S. Robb, S. McCallum, A. Koptioug, and D. J. Lurie, Recent developments in combining LODESR imaging with proton NMR imaging, *Phys. Med. Biol.* **43,** 1851–1855 (1998).